

Article

Single Inductor-Multiple Output DPWM DC-DC Boost Converter with a High Efficiency and Small Area

Young Jun Park¹, Zaffar Hayat Nawaz Khan¹, Seong Jin Oh¹, Byeong Gi Jang¹, Nabeel Ahmad¹, Danial Khan¹, Hamed Abbasizadeh¹, Syed Adil Ali Shah¹, Young Gun Pu¹, Keum Cheol Hwang¹ , Youngoo Yang¹, Minjae Lee² and Kang Yoon Lee^{1,*}

¹ College of Information and Communication Engineering, Sungkyunkwan University, Suwon 16419, Korea; pyj88@skku.edu (Y.J.P.); zaffar@skku.edu (Z.H.N.K.); geniejazz@skku.edu (S.J.O.); seeys17@skku.edu (B.G.J.); nabeel8@skku.edu (N.A.); danialkhan@skku.edu (D.K.); hamed@skku.edu (H.A.); adilshah@skku.edu (S.A.A.S.); hara1015@naver.com (Y.G.P.); khwang@skku.edu (K.C.H.); yang09@skku.edu (Y.Y.)

² School of Electrical Engineering and Computer Science, Gwangju Institute of Science and Technology, Gwangju 61005, Korea; minjae@gist.ac.kr

* Correspondence: klee@skku.edu; Tel.: +82-31-299-4954

Received: 1 March 2018; Accepted: 20 March 2018; Published: 23 March 2018



Abstract: In this paper, a small-area and high-efficiency single-inductor multiple output (SIMO) boost converter with digital pulse-width modulation (DPWM) is proposed. The DPWM comprises a delay line using interlaced hysteresis delay cells (IHDCs) that occupy a small area while consuming a low power amount. These proposed IHDCs are applied to replace the conventional delay cells of the prior works for both the power and area reductions. Regarding the DC-DC converter, this technique comprises fewer digital blocks in the feedback path compared with the conventional DC-DC converter, and the DPWM architecture uses IHDCs. The purpose of the digital limiter block is to concede some helpful code for the DPWM. The IHDC topology used for delay in DPWM is of the simplest architecture. The high-side power switch gate drivers need individual phases which are generated by phase control. The Complementary Metal Oxide Semiconductor (CMOS)-fabrication process is 55 nm, with a standard supply voltage of 1.8 V and outputs of 2.2 and 2.4 V. The chip area is approximately $170 \times 190 \mu\text{m}$ and its efficiency is 94.4%.

Keywords: DC-DC converter; digital pulse width modulation; interlaced hysteresis delay cells (IHDCs)

1. Introduction

The role of an efficient DC-DC converter in Internet of Things (IoTs) applications and electronic devices is important, while highly efficient power-management units are required for any electronic device in which the battery voltage is higher than the supply voltage. For today's electronic systems, an enhancement of the regulatory performance and the area efficiency are required [1]. Numerous research works on the DC-DC converter have been reported, with the focus of some of them comprising small-sized, low-cost, low-power-consuming modern portable electronic devices. These converters are usually equipped with an off-chip inductor for maximum efficiency, and it is expected that they can offer multiple output-voltage levels, which is why they are called single-inductor multiple output (SIMO) DC-DC converters. Due to advancement of circuit technology, the research area of the single-output concept has become saturated; however, several pieces of research have been completed in the area of analog-controller SIMO DC-DC converters as well. Also, system

stability, poor cross regulation and flexibility are the main issues of SIMO converters to achieve excellent performance [2–6]. Studies of the digital-controller converters can be found in [7,8], while the field-programmable gate array (FPGA), microcontrollers, and compact reconfigurable input output (cRIO) play key roles in the operation of the corresponding digital controller. In most DC-DC converters, a digital control is employed for the external microcontrollers, FPGAs, and cRIO modules [9,10]. By contrast, the designed on-chip digital compensator of this paper occupies a small area.

The conventional SIMO DC-DC Converter is shown in Figure 1. Usually conventional SIMO DC-DC converter has large area because of several analog-to-digital converters (ADCs), error amplifiers, counters, memory components, and filter capacitors. In addition, when the switching frequency is low, the inductance will be high, which causes a large area. Along with other SIMOs, in [11,12] also, the same number of ADCs and outputs are used. In contrast, in this work, no counter and error amplifiers are used except for one bandgap reference (BGR).

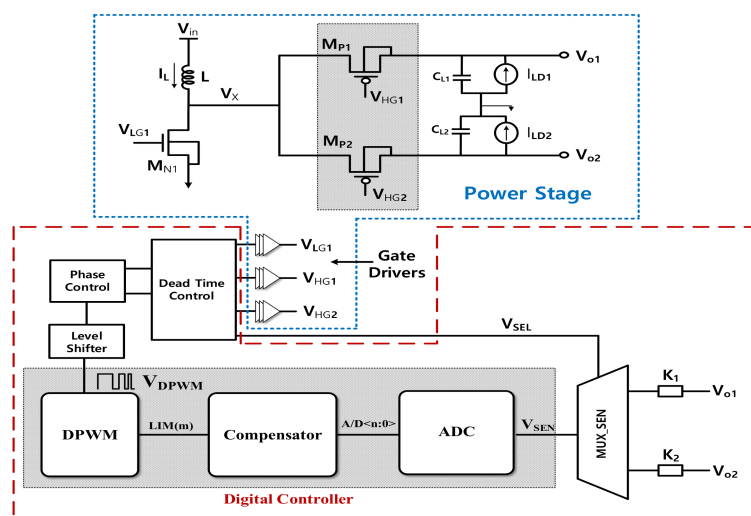


Figure 1. Conventional block diagram of a digitally controlled single-inductor multiple output (SIMO) DC-DC converter.

The issues of the SIMO DC-DC converter were studied. Poor cross-load regulation, line regulation, a low current capability, and a large ripple are the major disadvantages of the SIMO converter compared with the conventional DC-DC converter, while the poor cross-load regulation and the line regulation are considered to be critical problems. To reduce the cross-regulation, various techniques have been presented [13–15]. Furthermore, the relationship between the cross-regulation and the load-transient response is close [15]. Upon the occurrence of a load transience, a current mismatch occurs between the inductor current and the total output-load current until the inductor current is settled by a feedback loop. During this time, the other outputs are affected by this unbalanced current that is caused by the output load transience.

Time-multiplexing is a basic approach in SIMO DC-DC converters. This concept is responsible for not allowing the outputs to couple with each other, which reduces the cross-regulation effectively [13, 16]. On the other hand, to add more outputs, the output power is reduced by multiple charging cycles per switching period in consequence and again the outputs require individual charging. To decrease the switching loss, ordered power distributive control (OPDC) has been proposed. The concept of power distributive approaches [14,17] decreases switching losses than the SIMO converters proposed in [13,16]. However, ADCs, digital controllers and counters, error amplifiers, external memories, reference voltage sources, large filter capacitors, and higher inductances that can lower switching frequencies require a large area. To avoid so many blocks, [18] presents smooth loop handover (SLH) technique, solving the problems of close loop performance in digitally controlled SIMO converters.

However, because of the use of a conventional delay cell in [18], the die area is very large. Also, the number of outputs of this architecture is limited up to two.

This work presents a SIMO DC-DC converter with an interlaced hysteresis delay cell (IHDC)-topology using digital pulse-width modulation (DPWM) that is highly efficient and comprises a small area; furthermore, the transistor sizes are smaller than those of the conventional delay cells [19]. In addition, the proposed architecture is extendable up to N outputs. DPWM plays a key role in terms of the digital controllers that convert the digital-limiter code to duty cycles. As area is a key factor of electronic devices, it was not used for both [18] and this work. In [16], a SIMO converter was designed having a share control loop in the analog domain. On the other hand, in this architecture feed-back control is used in the digital domain based on loop handover (LHO) topology.

In [20,21], the scheme of SLH is used only in analog domain, but in [22], the scheme can apply in SIMO architectures with a digital control. This scheme is the best solution for the issues of the close loop that occur in DPWM SIMO DC-DC converters.

The rest of the paper continues as follows: the architectures of the DPWM SIMO DC-DC converter and the proposed IHDCs based on DPWM are explained in Section 2. Section 3 shows the experimental and measurement results. Finally, brief conclusions are given in Section 4.

2. Architecture of DPWM SIMO DC-DC Converter

The proposed configuration of the present paper is composed of an IHDC-based DPWM, a Type-III digital compensator, a SIMO power stage, scaling and multiplexing, and a digital feedback controller, as shown in Figure 2. In the proposed technique, the use of IHDCs has advantage of large delay, low power loss and small size over conventional delay cells; this IHDC-based DPWM scheme is explained in Section 2.2.2. The proposed architecture is designed for two different output voltages, so the output fluctuations depend on the instantaneous energy present in the inductor and the feedback-resistance values for each output.

The proposed architecture does not require many reference voltages (V_{ref}); it has only one (V_{ref}). To get different feedback voltage, the value of the feedback resistances should be different. The fluctuation can be decreased, if the amount of inductor charge is enough before the load changes at V_{o1} . On the other hand, in the case of an inadequate energy value, because of different resistance values, the inductor must be charged and discharged for a relatively long duration of time.

When the power transistor M_{N1} is on, the inductor is charged. In the next phase, however, the M_{N1} is off and the M_{P1} is on for the transferal of the energy that is stored in the inductor to V_{o1} ; furthermore, this cycle is repeated for V_{o2} as well, and a detailed description with a timing diagram is provided. This phenomenon of the control stage is explained in Section 2.2.

V_{o1} and V_{o2} are provided as the multiplexer (Mux_SEN) inputs. The term fs/n selects each output, the fs represents switching frequency while n shows the number of outputs, which is converted by ADC into digital data. After that it is fed to Type-III digital compensator.

To avoiding overlapping, the digital limiter masks are designed to allow only the data that can be used, while the rest of the data are masked. These data can be converted into duty cycle by the DPWM. At the beginning, the LHO block is protected from affected input data provided by the DPWM. After a pre-specified time, the loop is completed in the tracking mode to achieve stability when the desired output-voltage levels are met. The clock divider helps to get fs/n frequency from the original source fs . The purpose of this action is to get a phase number that is the same number of outputs. Gate drivers are fed by phase control which is connected to P-type Metal Oxide Semiconductor (PMOS) power transistors M_{P1} and M_{P2} , while the V_{LG1} bypasses the phase controller.

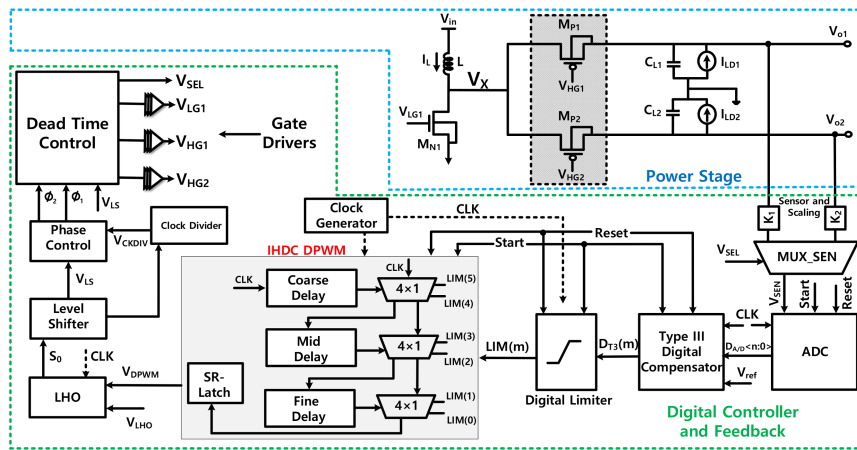


Figure 2. Proposed SIMO DPWM DC-DC converter based on interlaced hysteresis delay cells (IHDCs).

Figure 3a shows the timing diagram for the power stage, where V_{LG1} is the M_{N1} driving signal with the time period T_s , and P_h is the phase-control signal with $T_{Ph} = 2(T_s)$. To keep the resistance minimum, widths (W) should be large like $(W_{MP1}, W_{MP2}) \geq 2 \times W_{MN1}$. The efficiency decreases by increasing the difference between the input and the output. To avoid a big difference, the input voltage should be slender, lower than the selected low output-voltage levels. The power transistor M_{N1} is switched on for a total of n times in one MP_n time period, where n is the number of outputs. The M_{N1} switched-on time is dictated by the controller CLK feedback depending on the previous voltage levels at the V_{o1} and V_{o2} outputs.

Figure 3b shows the timing diagram of the digital stage. At the start, $D_{T3}(m)$, $LIM(m)$ and inverted DPWM are reset. After the start signal they become active. Until the LHO signal is low, any output $D_{T3}(m)$ from the digital stage is masked, as shown with the masking period. Ideally, the DPWM resolution should be greater than or equal to that of the Type-III digital compensator, which can be greater than or equal to that of the ADC to avoid limit cycling.

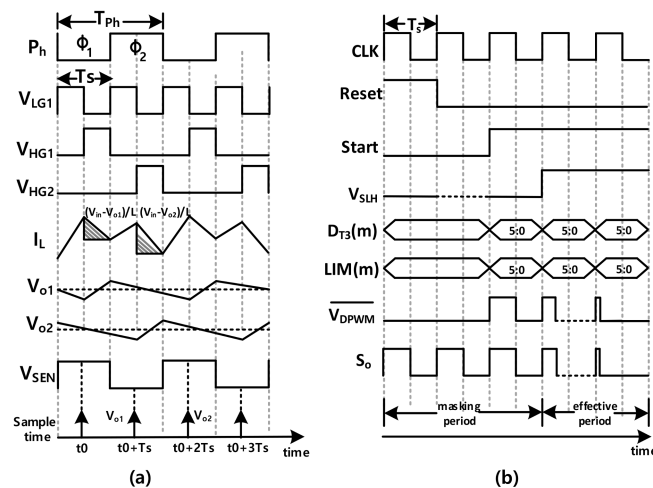


Figure 3. Detailed timing diagram of the proposed DPWM SIMO DC-DC converter: (a) timing diagram of the power stage, and (b) timing diagram of the digital-control stage.

To save area and power consumption, a six-bit resolution is added to this architecture. In this work, to overcome the redundancy of the composter, ADC and DPWM, one control loop is shared by both outputs which has a benefit of low cost and small area. For $V_{SEL} = 0$, the feedback for V_{o1} output

is processed through the control stage at phase Φ_1 . Likely, for $V_{SEL} = 1$, the feedback for V_{o2} output is processed through the control stage at phase Φ_2 .

Both feedback output voltages take a sampling duration $1/(f_s/n) = (1/(5 \text{ MHz}/2)) = 400 \text{ ns}$. A scaled-down V_{o1} is sampled at $t_0, t_0 + 2T_s, t_0 + 4T_s, \dots$, and V_{o2} is sampled at $t_0 + T_s, t_0 + 3T_s, t_0 + 5T_s, \dots$. For excellence accuracy, the control design band width which is equal to 5MHz is used. For gains these equations can be used $K_1 = V_{ref}/V_{o1}$, $K_2 = V_{ref}/V_{o2}$.

2.1. SIMO Power Stage

Figure 4a presents the SIMO power stage. When M_{N1} is on and M_{P1} and M_{P2} are off, the inductor L charges with the input voltage $(V_{in})/L$ slope, whereas when M_{P1} is on at the rate of $(V_{in} - V_{o1})/L$, it discharges together with the V_{in} to V_{o1} . In the second phase, the slope of V_{o2} is calculated as $(V_{in} - V_{o2})/L$; therefore, the discharging of the inductor energy is alternatively transferred to the available outputs. The difference between the input and output voltages is inversely proportional to efficiency. So, a small difference is preferred; for this purpose output voltages should be chosen that are slender greater than the input. The switched-on time of the M_{N1} is dictated by the controller feedback depending on the previous voltage levels at the V_{o1} and V_{o2} outputs. V_{o1}/K_1 and V_{o2}/K_2 are scaled-down signals from the sensors K_1 and K_2 . ADC is fed by Mux_SEN V_{SEN} that are connected to ADC as an input. By energy transfer, the voltage ripple at V_{o1} increases and then decreases by energy shifting to the next output. The simulation results are shown in Figure 4b.

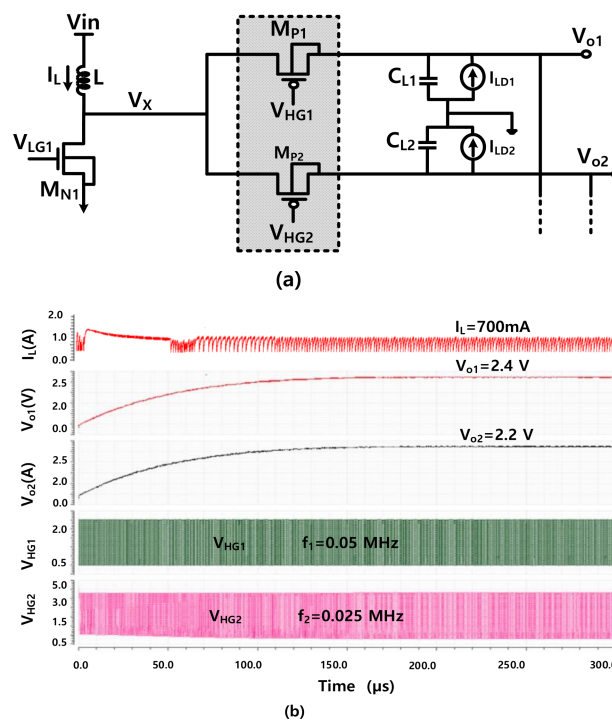


Figure 4. Power stage of SIMO DC-DC converter: (a) schematic of the power stage, and (b) simulation results of the power stage.

2.2. SIMO Control Stage

2.2.1. Digital Limiter

Only the data that must result in a duty-cycle in the range from 5–90% are allowed by the digital limiter, while the rest of the data are masked. A six-bit word Hi-Limit and Lo-Limit set the digital-limiter window. Figure 5 show the flowchart and effective region of digital limiter.

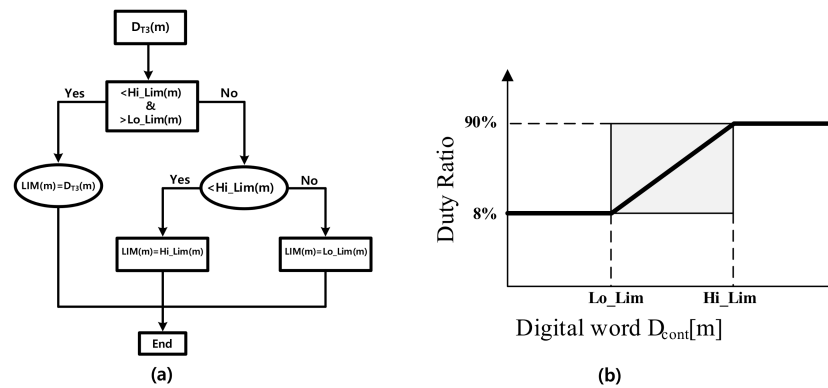


Figure 5. Digital limiter of a SIMO DC-DC converter: (a) flowchart of the digital limiter (b) effective region of the digital limiter.

As the input word, the Type-III digital compensator fed $D_{T3}(m)$ is compared to the predefined Hi-Limit and Lo-Limit. The output $LIM(m)$ will be equal to input by inserting the input word in the Limit. On the other hand, if the input is higher than the Hi-Limit or less than the Lo-Limit, the output becomes either the Hi-Limit or the Lo-Limit, respectively, through the ignoring of the input word.

2.2.2. Proposed IHDC-Based DPWM.

The DPWM block is shown in Figure 6a. The advantages of this architecture are that it does not require any counter and it comprises small-area delay cells. The data that is allowed by the digital limiter is converted to the duty cycle by DPWM. In this architecture, the topology of IHDC greatly reduces the area of DPWM. To avoid loading effect an extra block is used.

In Figure 6b Interlaced Hysteresis Delay Cell architecture is given. The series M1-M8 plays a key role for delay implementation. The series M9-M12 is responsible for floating node charges/discharges. Node “a” is connected to a, b to b, c to c, d to d and node e is connected to e. Figure 6c shows the timing diagram of the proposed IHDC, while Figure 6d shows the simulated delay at each IHDC node. Suppose IN is high which starts to low so M1 is ON and “a” starts to high. When M8 is ON, b starts to low.

When M2 is ON, c starts high which turns on M7 and discharges OUT to ground. To remove the fluctuation in the delay, we can a buffer at output of the delay cell.

In this architecture when the signal changes, there is no short-circuit available. It is because of switching of PMOS and N-type Metal Oxide Semiconductor (NMOS) individually. When the transition is for long duration, the power consumption in the Inverter (INV) is controlled by the short-circuit current. Therefore, the total power is largely reduced compared with the conventional delay cells. Furthermore, there are two paths for current flow; the transistors put the charge in the same path, which results in saving the leakage current. To increase the amount of shared charges and delay, more transistors should be added in a path.

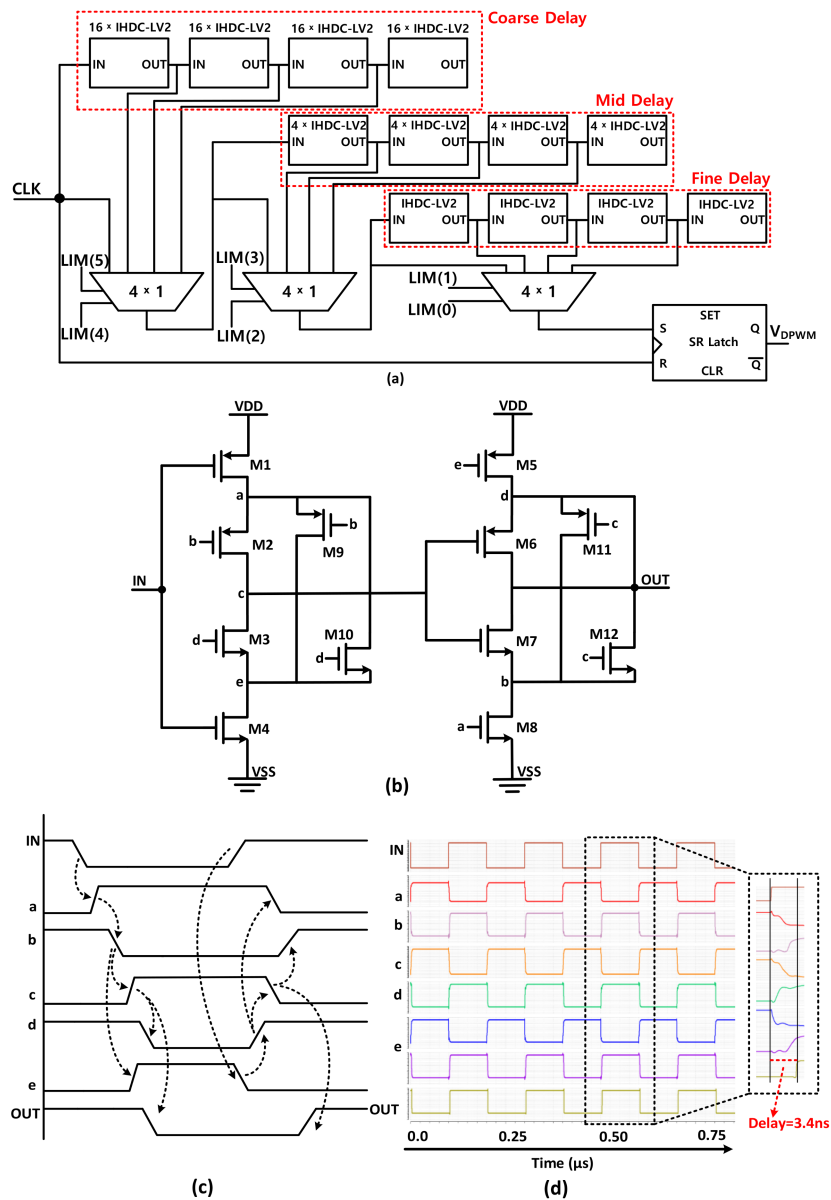


Figure 6. Proposed DPWM architecture. (a) Six-bit DPWM, (b) proposed IHDC-LV2, (c) timing diagram of the proposed IHDC, and (d) simulated delay at each node of the proposed IHDC.

2.2.3. Comparisons of Delay Cells.

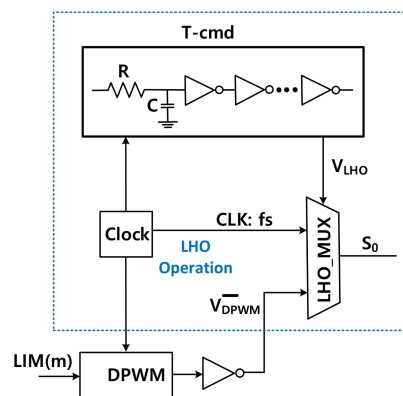
Table 1 shows the comparison results of the various delay techniques in a 55-nm CMOS process. In [23,24] the INV and AND logic gate take power in the range of 90-to-80 μ W. The size is because of 800 transistors. In [25], the power of the cascaded hysteresis delay cell (CHDC) is 84% less than INV. Similarly, its area is 70% less than INV. The process, voltage and temperature (PVT) variations, however, are two times the conventional delay because of several weakly internal nodes. The application of extra delay cells can overcome delay variation that can increase power and area. Because of PVT, there will be some noise. It can be reduced if the internal nodes of IHDCs are derived perfectly. IHDCs can be used instead of many INV or logic gates to save area and power.

Table 1. Performance comparisons of different delay cells.

Technique	Period	Power	Delay Cell Number	Transistor Count	PVT Variation
INV [23]	9.96 ns	93.8 μ W	402	804	1.14
AND [24]	10.12 ns	82.5 μ W	161	966	1.21
CHDC [25]	9.97 ns	15.3 μ W	2	244	2.27
IHDC-LV2	10.08 ns	82.6 μ W	41	492	1.22

2.2.4. Loop Handover (LHO).

The proposed LHO block diagram shown in Figure 7. The LHO block was used to solve the problem of the initial transients and to improve the close-loop performance; also, its usage reduced the power consumption, thereby improving the overall efficiency of the converter. The conventional soft-start circuit requires many analog errors, amplifiers, comparators, and capacitor banks. A capacitor bank typically requires the same number of capacitors and bit numbers in the trim-bit control, and this ultimately increases the complexity and the layout area.

**Figure 7.** Detailed diagram of a loop handover (LHO).

However, proposed LHO requires a DPWM with inverter at its output, frequency generation clock and a multiplexer (LHO_MUX). Both the DPWM and the LHO_MUX use the clock simultaneously.

The digital word from the digital limiter is input into the DPWM block to generate the varying duty cycles proportional to the output voltages of the DC-DC converter. During the initial startup, this duty-cycle variation is random and causes instability. To overcome this issue, the DPWM signal is first inverted and masked for a predetermined time, followed by its assignment by the timing-command generator (T-cmd) block. The switching-frequency clock (CLK) source is used in a star manner to reduce the latency. The LHO is accomplished using the inverted DPWM output, T-cmd, and LHO_MUX; the DPWM, T-cmd, and LHO_MUX blocks use the same available CLK. The control-signal V_{LHO} selects the switching source with a 50% duty ratio for 20 μ s.

2.2.5. Phase Control.

The phase-control block generates the complementary phases for the gate drivers of the high-side power switches. Onward, the output receives the adjacent signal, at least one output signal is required for the supply voltage. Figure 8a shows the block diagram of the phase control for N-outputs.

The following two signals can drive the phase-control block: the level shifter signal and the clock divider signal that is used for controlling purpose. Figure 8b shows a timing diagram of the phase-control logic for N-outputs.

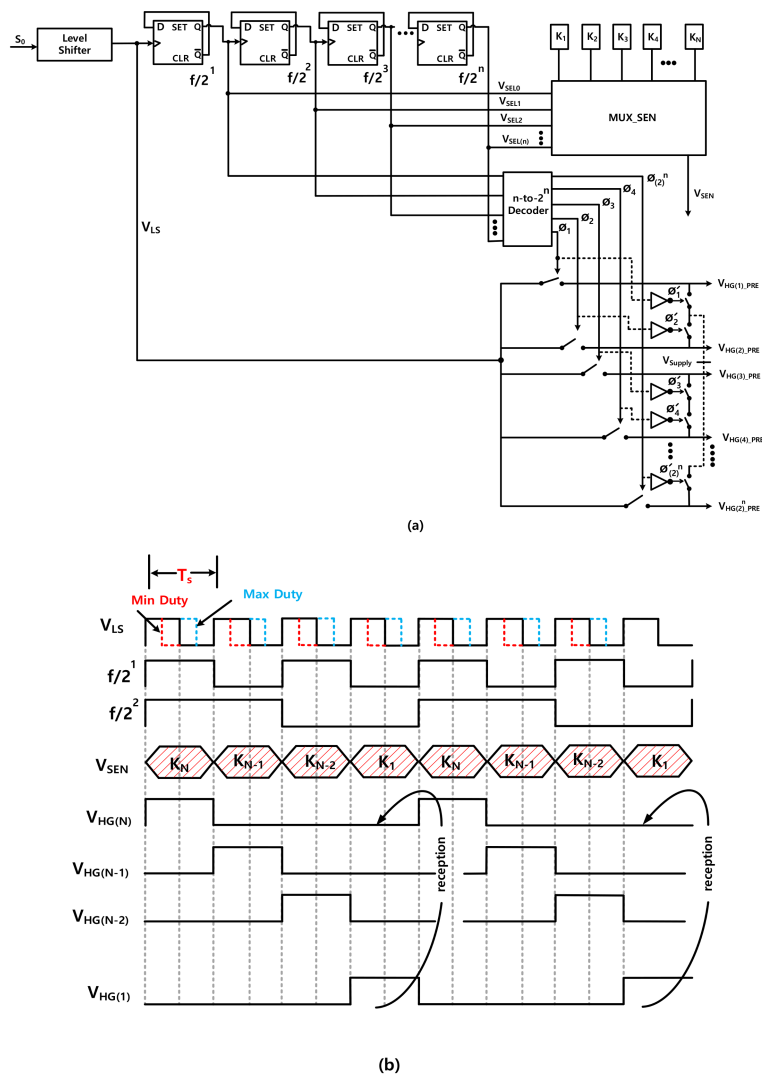


Figure 8. (a) Phase-control logic for N-outputs. (b) Timing diagram for N-outputs.

3. Experimental Result

The layout of the proposed SIMO DC-DC converter that is shown in Figure 9 consists of the proposed digital controller, the DPWM, the digital limiter, gate drivers, the SIMO power stage, and the phase-control blocks. The total active area is $170 \times 190 \mu\text{m}$.

Figure 10 shows the top simulation result and the measured efficiency with the input voltage of 1.8 V and the output-voltage values of 2.2 and 2.4 V, and the measured efficiency is 94.4%.

Figure 11a shows the measured output voltage of V_{o1} . The measured voltage is 2.38 V with the peak-to-peak ripple of 25 mV. The single box resolution of the oscilloscope was set to be 1 V. The decaying voltage was restored by the feedback loop after the sensing by the output sense circuitry, as can be seen in the measurement. Figure 11b shows the measured output voltage of V_{o2} , where a constant oscilloscope-measured voltage of 2.19 V is shown. The peak-to-peak ripple for this case was measured to be 20 mV.

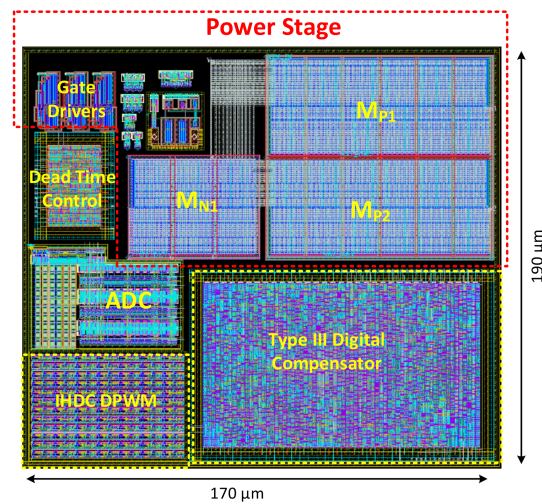


Figure 9. Layout of the proposed DPWM SIMO DC-DC converter.

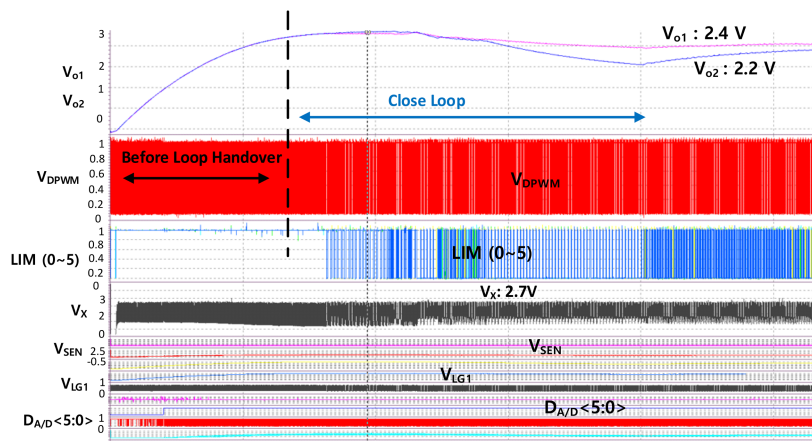


Figure 10. Top simulation result of the proposed DPWM SIMO DC-DC converter.

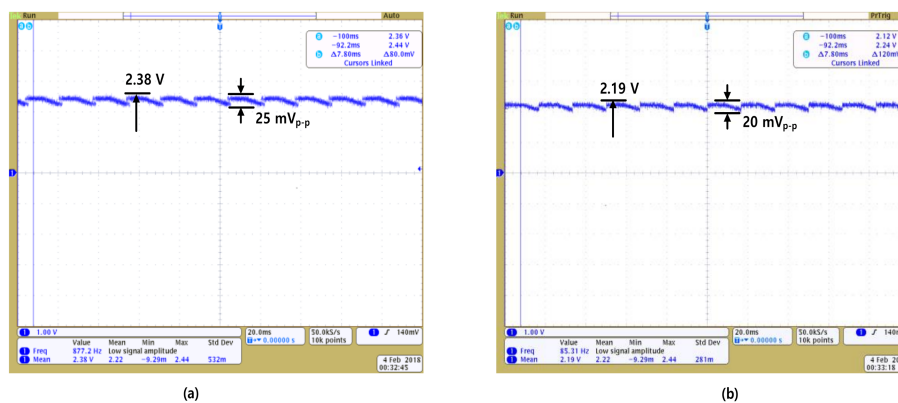


Figure 11. Measurement results for the outputs of the proposed SIMO DC-DC converter (a) V_{o1} (b) V_{o2} .

Figure 12 shows the load and cross regulations for the V_{o1} and V_{o2} , respectively. The load current was changed from 10 to 80 mA in both cases. The output voltage was reduced by 20 mV for V_{o1} at the full load of 80 mA. The output voltage for the V_{o2} was reduced by 15 mV at the full load of 80 mA.

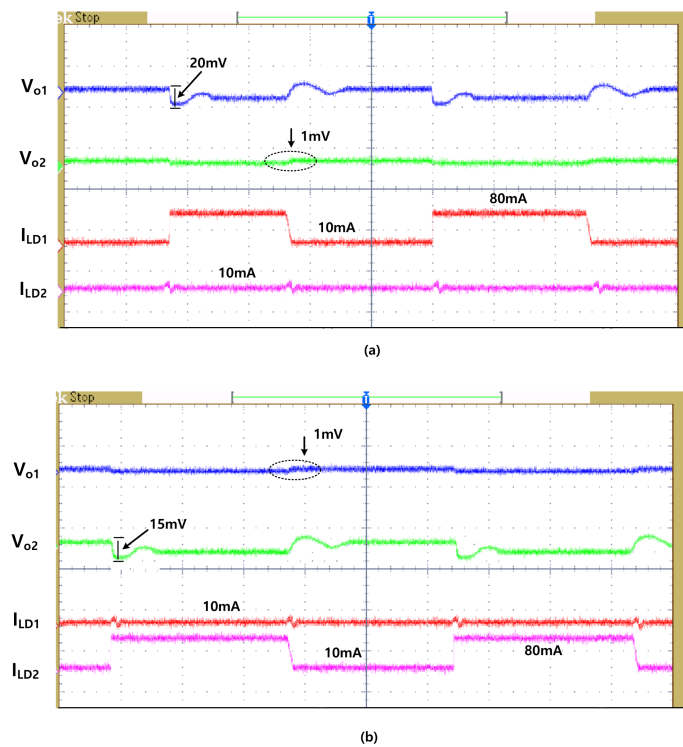


Figure 12. Measurement results for load and cross regulation (a) at load current I_{LD1} from 10 to 80 mA (b) load current I_{LD2} from 10 to 80 mA.

Table 2 shows the comparison of this work with the previous works. A very small area of 0.0323 mm^2 and an efficiency of 94.4% are the main differentiate points of this work; compared with the other techniques, this technique required fewer digital-control blocks, and IHDCs which occupy a smaller area and consume less power are used for this architecture. In addition, the compensator of this design is fully integrated, on the other hand, the controllers in the reference works need the FPGA or the cRIO.

Table 2. Performance comparison with prior works.

Parameters	[7]	[8]	[9]	[18]	[11]	This Work
Process	0.35 μm	130 nm	FPGA/cRIO	55 nm	EP1C3T	55 nm
Modulation	DPWM	PWM	PWM	DPWM	DPWM	DPWM
Buck/Boost	Boost/Buck	Boost	Buck	Boost	Buck	Boost
Input Voltage	3.3 V	1.5 V	5 V	1.8 V	2.5–5 V	1.8 V
Out Voltages	3.63 V, 2.02 V, 1.55 V	2.5 V, 1.8 V	1.0 V, 1.5 V	2 V, 2.2 V	1.5 V, 1.25 V, 1 V	2.4 V, 2.2 V
Counters	N/A	Needed	N/A	N/A	N/A	N/A
LHO	-	-	-	Yes	-	Yes
Output Power	19 mW, 64.6 mW, 32 mW	125 mW, 180 mW	320 mW, 360 mW	89 mW, 107 mW	150 mW, 150 mW	85 mW, 104 mW
Cross Regulation (mV/mA)	-	0.26@2.5 V and 125 mW, 0.12@1.8 V and 180 mW	0.02@1.0 V and 320 mW, 0.01@1.5 V and 360 mW	-	-	0.01@2.4 V and 85 mW, 0.01@2.2 V and 104 mW
Efficiency	83.5%	-	-	94.3%	-	94.4%
Area (mm^2)	2.72	1	N/A	0.06	-	0.0323

4. Conclusions

A small-area and high-efficiency DPWM DC-DC converter for which the IHDC topology is applied, where a shared control-loop was employed in the 55-nm process, is proposed in this paper. Regarding the proposed converter, the area and the power consumption were reduced using the IHDCs in the DPWM architecture with smaller area of the Type-III digital-compensator including the memory blocks, which is $82 \times 130 \mu\text{m}$. To solve the area issue, the IHDCs DPWM is the simplest topology. To regulate several outputs, only one control path is needed. Also, the design of the digital limiter ensures the validity of the data that are used for the DPWM block. Counters are also avoided to reduce the overall power consumption. The converter has a smaller inductor of 600 nH and filtering capacitor of 2 μF . The converter input is 1.8 V, its outputs are 2.2 and 2.4 V, and the measured efficiency is 94.4%. The total active area is $170 \times 190 \mu\text{m}$.

Acknowledgments: This work was supported by the R&D program of MOTIE/KEIT. (10080364, Development of a High Efficient Energy Hub System for IoT Devices). This work was supported by the National Research Foundation of Korea (NRF) grant funded by the Korean government (MSIP) (2014R1A5A1011478).

Author Contributions: Kang-Yoon Lee guided and directed the authors for this work. Young-Jun Park and Zaffar Hayat Nawaz Khan studied, proposed and designed the overall architecture of SIMO DPWM DC-DC Boost Converter. They wrote the paper. Seong Jin Oh, Byeong Gi Jang, Hamed Abbaszadeh and Syed Adil Ali Shah contributed in making the layout of the proposed architecture. Nabeel Ahmad guided in the digital part of the architecture and measurements. Young Gun Pu performed the measurements with Young-Jun Park, Zaffar and Danial Khan. Keum Cheol Hwang, Youngoo Yang and Minjae Lee designed the related top architecture.

Conflicts of Interest: The authors declare no conflict of interest.

References

1. Qian, Z.; Abdel-Rahman, O.; Al-Atrash, H.; Batarseh, I. Modeling and control of three-port DC/DC converter interface for satellite applications. *IEEE Trans. Power Electron.* **2010**, *25*, 637–649. [[CrossRef](#)]
2. Huang, C.-Y.; Chen, Y.-C.; Tsai, C.-H. Integrated single-inductor dual-output DC-DC converter with power-distributive control. In Proceedings of the 2013 IEEE International Symposium on Next-Generation Electronics (ISNE), Kaohsiung, Taiwan, 25–26 February 2013; pp. 33–36.
3. Nakase, Y.; Hirose, S.; Onoda, H.; Ido, Y.; Shimizu, Y.; Oishi, T.; Kumamoto, T.; Shimizu, T. 0.5 V Start-Up 87% Efficiency 0.75 mm² On-Chip Feed-Forward Single-Inductor Dual-Output (SIDO) Boost DC-DC Converter for Battery and Solar Cell Operation Sensor Network Micro-Computer Integration. *IEEE J. Solid State Circuits* **2013**, *48*, 1933–1942. [[CrossRef](#)]
4. Chen, C.-M.; Hsu, K.-H.; Hung, C.-C. Freewheel charge-pump controlled single-inductor multiple-output step-up DC-DC converter. *Analog Integr. Circuits Signal Process.* **2013**, *74*, 215–225. [[CrossRef](#)]
5. Ko, Y.; Jang, Y.; Han, S.-K.; Lee, S.-G. Load-Balance-Independent High Efficiency Single-Inductor Multiple-Output (SIMO) DC-DC Converters. *J. Semicond. Technol. Sci.* **2014**, *14*, 300–312. [[CrossRef](#)]
6. Chen, P.-H.; Fan, P.M.-Y. An 83.4% Peak Efficiency Single-Inductor Multiple-Output Based Adaptive Gate Biasing DC-DC Converter for Thermoelectric Energy Harvesting. *IEEE Trans. Circuits Syst. I Regul. Pap.* **2015**, *62*, 405–412. [[CrossRef](#)]
7. Jia, J.; Leung, K.N. “Digital-control single-inductor triple-output DC-DC converter with pre-sub-period inductor-current control. *IEEE Trans. Power Electron.* **2012**, *27*, 2028–2042. [[CrossRef](#)]
8. Zhang, Y.; Ma, D. Digitally controlled integrated pseudo-CCM SIMO converter with adaptive freewheel current modulation. In Proceedings of the Twenty-Fifth Annual IEEE Applied Power Electronics Conference and Exposition (APEC), Palm Springs, CA, USA, 21–25 February 2010; pp. 284–288.
9. Dasika, J.D.; Bahrani, B.; Saeedifard, M.; Karimi, A.; Rufer, A. Multivariable control of single-inductor dual-output buck converters. *IEEE Trans. Power Electron.* **2014**, *29*, 2061–2070. [[CrossRef](#)]
10. Lee, A.T.; Sin, J.K.; Chan, P.C. Scalability of quasi-hysteretic fsm-based digitally controlled single-inductor dual-string buck LED driver to multiple strings. *IEEE Trans. Power Electron.* **2014**, *29*, 501–513. [[CrossRef](#)]
11. Trevisan, D.; Mattavelli, P.; Tenti, P. Digital control of single-inductor multiple-output step-down DC-DC converters in CCM. *IEEE Trans. Ind. Electron.* **2008**, *55*, 3476–3483. [[CrossRef](#)]

12. Shen, Z.; Chang, X.; Wang, W.; Tan, X.; Yan, N.; Min, H. Predictive digital current control of single-inductor multiple-output converters in CCM with low cross regulation. *IEEE Trans. Power Electron.* **2012**, *27*, 1917–1925. [[CrossRef](#)]
13. Ma, D.; Ki, W.-H.; Tsui, C.-Y. A pseudo-CCM/DCM SIMO switching converter with freewheel switching. *IEEE J. Solid State Circuits* **2003**, *38*, 1007–1014.
14. Le, H.-P.; Chae, C.-S.; Lee, K.-C.; Wang, S.-W.; Cho, G.-H.; Cho, G.-H. A single-inductor switching DC-DC converter with five outputs and ordered power-distributive control. *IEEE J. Solid State Circuits* **2007**, *42*, 2706–2714. [[CrossRef](#)]
15. Lu, D.; Qian, Y.; Hong, Z. An 87% Peak Efficiency DVS-capable Single-Inductor 4-Output DC-DC Buck Converter with Ripple-based Adaptive Off-time Control. In Proceedings of the 2014 IEEE International Solid-State Circuits Conference Digest of Technical Papers (ISSCC), San Francisco, CA, USA, 9–13 February 2014; pp. 82–83.
16. Ma, D.; Ki, W.-H.; Tsui, C.-Y.; Mok, P.K. Single-inductor multiple-output converters with time-multiplexing control in discontinuous conduction mode. *IEEE J. Solid State Circuits* **2003**, *38*, 89–100.
17. Huang, M.-H.; Chen, K.-H. Single-inductor multi-output (SIMO) DC-DC converters with high light-load efficiency and minimized cross-regulation for portable devices. *IEEE J. Solid State Circuits* **2009**, *44*, 1099–1111. [[CrossRef](#)]
18. Hayder, A.S.; Park, Y.; Kim, S.Y.; Pu, Y.G.; Yoo, S.S.; Yang, Y.; Lee, M.; Hwang, K.C.; Lee, K. Digitally Controlled Single Inductor Multiple Output Synchronous DC-DC Boost Converter with Smooth Loop Handover using 55 nm Process. *J. Power Electron.* **2017**, *17*, 821–834. [[CrossRef](#)]
19. Yu, C.; Chung, C.; Yu, C.; Lee, C. A Low-Power DCO Using Interlaced Hysteresis Delay Cells. *IEEE Trans. Circuit Syst.* **2012**, *59*, 673–677.
20. Hayder, A.S.; Kim, H.; Kang, J.-H.; Lee, K.-Y. 3.7 V high frequency DC-DC synchronous boost converter with smooth loop handover. In Proceedings of the 14th International Symposium on Communications and Information Technologies (ISCIT), Incheon, Korea, 24–26 September 2014; pp. 191–194.
21. Hayder, A.S.; Park, H.-G.; Kim, H.; Lee, D.-S.; Abbasizadeh, H.; Lee, K.-Y. A Single Inductor Dual Output Synchronous High Speed DC-DC Boost Converter using Type-III Compensation for Low Power Applications. *IEIE Trans. Smart Process. Comput.* **2015**, *4*, 44–50. [[CrossRef](#)]
22. Hayder, A.S.; Kim, S.Y.; Abbasizadeh, H.; Lee, K.Y. Loop-handover technique for digitally controlled multiple-output dc-dc converters. *IET Electron. Lett.* **2016**, *52*, 1889–1891. [[CrossRef](#)]
23. Chung, C.C.; Lee, C.Y. An all-digital phase-locked loop for highspeed clock generation. *IEEE J. Solid State Circuits* **2003**, *38*, 347–351. [[CrossRef](#)]
24. Sheng, D.; Chung, C.C.; Lee, C.Y. An ultra-low-power and portable digitally controlled oscillator for SoC applications. *IEEE Trans. Circuits Syst. II* **2007**, *54*, 954–958. [[CrossRef](#)]
25. Hsu, S.Y.; Yu, J.Y.; Lee, C.Y. A sub-10 μ W DCO based on HDC topologies for WBAN applications. *IEEE Trans. Circuits Syst. II Express Briefs* **2010**, *57*, 951–955. [[CrossRef](#)]



© 2018 by the authors. Licensee MDPI, Basel, Switzerland. This article is an open access article distributed under the terms and conditions of the Creative Commons Attribution (CC BY) license (<http://creativecommons.org/licenses/by/4.0/>).